Accepted Manuscript

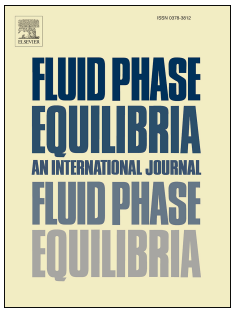

A stable algorithm for calculating phase equilibria with capillarity at specified moles, volume and temperature using a dynamic model

Jisheng Kou, Shuyu Sun

PII: S0378-3812(17)30356-4

DOI: 10.1016/j.fluid.2017.09.018

Reference: FLUID 11590

To appear in: *Fluid Phase Equilibria*

Received Date: 1 May 2017

Revised Date: 18 September 2017

Accepted Date: 20 September 2017

Please cite this article as: J. Kou, S. Sun, A stable algorithm for calculating phase equilibria with capillarity at specified moles, volume and temperature using a dynamic model, *Fluid Phase Equilibria* (2017), doi: 10.1016/j.fluid.2017.09.018.

A STABLE ALGORITHM FOR CALCULATING PHASE EQUILIBRIA WITH CAPILLARITY AT SPECIFIED MOLES, VOLUME AND TEMPERATURE USING A DYNAMIC MODEL *

JISHENG KOU† AND SHUYU SUN‡

Abstract. Capillary pressure can significantly affect the phase properties and flow of liquid-gas fluids in porous media, and thus, the phase equilibrium calculation incorporating capillary pressure is crucial to simulate such problems accurately. Recently, the phase equilibrium calculation at specified moles, volume and temperature (NVT-flash) becomes an attractive issue. In this paper, capillarity is incorporated into the phase equilibrium calculation at specified moles, volume and temperature. A dynamical model for such problem is developed for the first time by using the laws of thermodynamics and Onsager's reciprocal principle. This model consists of the evolutionary equations for moles and volume, and it can characterize the evolutionary process from a non-equilibrium state to an equilibrium state in the presence of capillarity effect at specified moles, volume and temperature. The phase equilibrium equations are naturally derived. To simulate the proposed dynamical model efficiently, we adopt the convex-concave splitting of the total Helmholtz energy, and propose a thermodynamically stable numerical algorithm, which is proved to preserve the second law of thermodynamics at the discrete level. Using the thermodynamical relations, we derive a phase stability condition with capillarity effect at specified moles, volume and temperature. Moreover, we propose a stable numerical algorithm for the phase stability testing, which can provide the feasible initial conditions. The performance of the proposed methods in predicting phase properties under capillarity effect is demonstrated on various cases of pure substance and mixture systems.

Key words. Phase equilibria; NVT flash; Phase stability; Capillarity; Thermodynamical modeling; Convex-concave splitting.

1. Introduction. Capillarity plays a very important role in multiphase systems arising from a number of oil reservoir and chemical engineering problems. Typically, a gas-oil reservoir involves liquid phase, gas phase as well as water phase [3, 6, 16]. Capillary pressure is one of the most significant driving forces in multi-phase flow in porous media, especially in fractured media; in fact, capillarity is frequently deemed as the leading mechanism of oil production in fractured reservoirs [3,10]. A few important parameters of physical processes in a porous medium, including relative permeability and residual saturations, are also significantly influenced by capillary pressure at a pore scale. In addition, capillarity is crucial for the counter-current flow [1], which is indeed driven by capillary pressure difference. Consequently, capillary pressure can substantially affect the flow and transport of the liquid and gas phases in a porous medium.

Phase equilibrium calculation is a key ingredient in modeling and simulation of multi-phase fluid systems. The physical properties of liquid and gas phases greatly impact the interfacial tension, which is one fundamental cause of capillarity. In the other hand, capillary pressure also significantly influences fluid behavior and phase equilibrium. In [36], it was shown that capillarity leads to significant changes in the phase densities and phase envelope of pure substances.

*This work is supported by National Natural Science Foundation of China (No.11301163). The authors cheerfully appreciate the generous support of the university research fund to the Computational Transport Phenomena Laboratory at KAUST.

†School of Mathematics and Statistics, Hubei Engineering University, Xiaogan 432000, Hubei, China.

‡Corresponding author. Computational Transport Phenomena Laboratory, Division of Physical Science and Engineering, King Abdullah University of Science and Technology, Thuwal 23955-6900, Kingdom of Saudi Arabia. Email: shuyu.sun@kaust.edu.sa.

In the phase equilibrium calculation, the selection of specified thermodynamical variables largely depends on the practical problems to be solved. NPT-flash accounts for the condition at specified pressure, temperature, and chemical composition [17, 18, 20]. Another alternative phase equilibrium state is determined under specified moles, volume, and temperature (the so-called NVT-flash). In [25], the volume-based thermodynamics was proposed to be used in equilibrium calculation; in [19], NVT-flash along with other specifications was discussed and formulated as minimization of a thermodynamic state function. The NVT-flash has been intensively studied recently [8, 9, 14, 21, 22, 28].

Recently, capillary pressure is involved in the phase equilibrium at the NPT conditions [26, 30, 33, 36, 37] since capillarity can significantly change phase properties. However, there are very few contributions on the NVT-flash calculation incorporating capillarity effect. As shown in this work, capillarity has a great effect on fluid behaviors and phase equilibria at specified moles, volume and temperature. Moreover, the NVT-flash involving capillarity is beneficial to accurately model the motion of multi-phase fluids in porous media since capillarity effect is generally viewed as one of the most important Darcy-scale phenomena resulting from the liquid-gas interfaces at the pore scale, and consequently, it is evidently an interesting and important issue.

In this paper, we consider the phase equilibrium calculation incorporating capillarity at specified specified moles, volume and temperature (i.e. NVT conditions). A dynamical model for such problem is rigorously derived through the laws of thermodynamics: by using the first law of thermodynamics, we first derive an entropy variation equation, which involves the work done by the capillary pressure; subsequently, the evolutionary equations of moles and volumes are derived by applying the second law of thermodynamics and Onsager's reciprocal principle [7]. To the best of our knowledge, it is the first time to develop such model, which can characterize the dynamical process from a non-equilibrium state to an equilibrium state in presence of capillarity effect at the NVT conditions. Especially, the proposed model has a feature that it has a set of unified formulations for both pure-substance and multi-component systems.

Thermodynamically stable numerical algorithms are more appreciated for simulating dynamical problems based on a realistic equation of state in recent years [11–14, 24, 29] since such methods can preserve the thermodynamical features that are desired for these problems. The convex-concave splitting approach is extensively used in numerical simulation of various gradient flows, especially phase-field models, in the literature, for example, [4, 32, 38]. This approach splits a free energy function into a summation of a convex part and a concave part; subsequently, the convex part is treated by the implicit time schemes, while the concave part is updated explicitly; consequently, it leads to unconditionally energy-stable time schemes (that is, any time step size can be used theoretically). In this work, a thermodynamically stable numerical algorithm is introduced to simulate the proposed dynamical model. This algorithm is designed through using the convex-concave splitting of the total Helmholtz energy, and thus, it is proved to preserve the second law of thermodynamics (also called entropy stability).

The phase stability analysis is usually used to determine whether a fluid system remains in a single phase or splits into two phases at specified conditions. For NPT flash involving capillary pressure, the stability analysis for multicomponent mixtures was developed in [33]. For the NVT-flash without capillarity, [22] has developed a phase stability testing approach, which is already employed to initialize the Newton's

minimization method in [8]. The phase stability analysis is required to provide the appropriate initial conditions, including initial values of moles and volumes. If this system stays in a single phase, then capillarity never occurs; otherwise, capillarity may take effect so that the phase properties may be significantly changed. In this work, we develop the phase stability analysis with capillarity at specified moles, volume and temperature using the entropy principle. Moreover, a stable numerical algorithm for the phase stability testing is developed through using the convex-concave splitting of the Helmholtz energy density.

The Kelvin equation, which reveals that the vapor pressure decreases with increasing interface curvature, has been applied for practical applications [6, 37]. It is assumed in Kelvin's equation that the phase equilibria occur between an ideal gas and an incompressible liquid, but this assumption may be no longer valid at the small pore sizes [37]. In numerical tests, we will compare the simulation results with Kelvin's equation and demonstrate the validity of numerical results.

The paper is organized as follows. In Section 2, we derive a dynamical model for phase equilibria involving capillarity at specified moles, volume, and temperature. In Section 3, a thermodynamically stable numerical algorithm is proposed based on the convex-concave splitting of the total Helmholtz energy. In Section 4, we derive a phase stability condition involving capillarity at specified moles, volume, and temperature, and develop a stable numerical method for phase stability analysis. In Section 5, we apply the proposed numerical algorithms on various cases of pure substance and mixture systems. At last, we summarize the main results in Section 6.

2. Dynamical model for phase equilibria involving capillarity. In this section, we first formulate the total Helmholtz free energy and capillary pressure, and subsequently, through using the first and second laws of thermodynamics and Onsager's reciprocal principle, we derive a dynamical model for phase equilibria in the presence of capillarity effect at specified moles, volume and temperature.

2.1. Total Helmholtz free energy. For a mixture composed of $M(M \geq 1)$ components, we denote by n_i the molar density of component i, and further denote the molar density vector by $\mathbf{n} = [n_1, n_2, \cdots, n_M]^T$. Let N_i represent the moles of component i, and then we denote the vector of moles by $\mathbf{N} = [N_1, \cdots, N_M]^T$. The phase equilibria of the mixture is considered under the constant overall volume (V^t), temperature (T) and overall mole numbers ($\mathbf{N}^t = [N_1^t, \cdots, N_M^t]^T$). We denote by $f(\mathbf{n})$ the Helmholtz free energy density of a homogeneous fluid, and its formulation can be found in Appendix A. For a two-phase system, we use V^G and V^L to represent the volumes of gas and liquid phases respectively, and we denote the moles of the gas phase by $\mathbf{N}^G = [N_1^G, \cdots, N_M^G]^T$ and moles of the liquid phase by $\mathbf{N}^L = [N_1^L, \cdots, N_M^L]^T$. Since the overall volume and overall moles are fixed, the following volume and mole constraints shall be satisfied

$$\mathbf{N}^G + \mathbf{N}^L = \mathbf{N}^t, \quad V^G + V^L = V^t. \tag{2.1}$$

The total Helmholtz free energy, denoted by F, can be expressed as

$$F = f(\mathbf{n}^G)V^G + f(\mathbf{n}^L)V^L \tag{2.2}$$

where

$$\mathbf{n}^G = \frac{\mathbf{N}^G}{V^G}, \quad \mathbf{n}^L = \frac{\mathbf{N}^L}{V^L}.$$

On account of the mass and volume constraints (2.1), F can be reduced into a function of $\mathbf{N}^G$ and V^G as $F(\mathbf{N}^G, V^G)$. The other choice of primal variables is also suggested in [8, 9, 35].

2.2. Capillarity. Due to capillarity effect, there exists a pressure difference at the contact between the gas and liquid phases, which is known as capillary pressure, denoted by p_c. Let p_G and p_L represent the pressures of gas and liquid phases respectively, and then the capillary pressure is expressed as

$$p_c = p_G - p_L. \tag{2.3}$$

For two-phase fluids in porous media, the capillary pressure is usually determined by the semi-empirical formulations, which are related to the saturation of a specified phase [3]. The capillarity pressure generally depends on various thermodynamical variables and physical properties, such as temperature, molar density, pore scale and contact angle. In the proposed model and numerical method of this work, the general capillarity effect can be taken into consideration. In numerical tests, we concentrate more on the capillary pressure given by a constant or calculated by the Young-Laplace equation and Weinaug–Katz correlation [39]. At the pore scale, the capillary pressure can be formulated by Young-Laplace equation [34]

$$p_c = \frac{2\sigma \cos\theta}{r}, \tag{2.4}$$

where σ stands for the interfacial tension, θ is the contact angle and r represents the pore radius. The contact angle is affected by the wettability. The interfacial tension σ can be provided by experimental data or calculated by a semi-empirical relation. In Appendix B, we describe the formulation of Weinaug–Katz correlation [39] for calculating the interfacial tension, which depends on compositions of two phases.

In order to apply the laws of thermodynamics, we need to describe the work done by the capillary pressure. For the pore scale, we consider a closed cylinder container with the fixed volume V^t under a constant temperature. We assume that this container is fully filled by a mixture with the overall moles, and this mixture may be split into the gas and liquid phases with a sharp interface, which occupy the volumes V^G and V^L, respectively, satisfying $V^G + V^L = V^t$. Correspondingly, the moles in the gas and liquid cells are denoted by $\mathbf{N}^G$ and $\mathbf{N}^L$, respectively. We use W to represent the total work done by the capillary pressure. When considering the work done by capillary pressure, we assume that for a specified time, the molar density is invariable but volume may change at this time. In this case, W has the form

$$\frac{dW}{dt} = -\int_I p_c \mathbf{u} \cdot \boldsymbol{\nu} dI, \tag{2.5}$$

where t is the time, I stands for the contact region between two phases, $\mathbf{u}$ is the velocity on the contact surface and $\boldsymbol{\nu}$ is a normal unit outward vector to I. For any given time, we assume that p_c has a unique value on the interface, and $\mathbf{u}$ is a constant vector in space, being parallel along cylinder towards from liquid to gas. The divergence theorem gives

$$\int_I \mathbf{u} \cdot \boldsymbol{\nu} dI - \int_A \mathbf{u} \cdot \boldsymbol{\nu} dA = 0, \tag{2.6}$$

where A is the cross-sectional area of this cylinder container. Consequently, assuming p_c is spatially constant, we derive

$$\frac{dW}{dt} = -p_c A\mathbf{u}\cdot\boldsymbol{\nu} = -p_c\frac{dV^G}{dt}. \tag{2.7}$$

For the scale of porous media, we assume that the contact surface is flat, so we still have

$$\frac{dW}{dt} = -p_c\frac{dV^G}{dt}. \tag{2.8}$$

2.3. Derivation of dynamical model. In [14], we have proposed a dynamical model for NVT-flash calculation without capillarity, which is derived from Fick's law of diffusion for multi-component fluids and the structure of Peng-Robinson equation of state. Different from the dynamical model in [14], the proposed model in this work is that capillarity effect is included in the NVT flash. The model derivation approaches in [14] cannot be extended to derive a model involving capillarity, so we propose a new derivation approach, which is based on the laws of thermodynamics and Onsager's reciprocal principle.

The total entropy S is a summation of two contributions [15]: $S = S_{\text{sys}} + S_{\text{env}}$, where S_{sys} is the entropy of the system, and S_{env} is the entropy of the environment. Let Q denote the heat transfer from the environment occurring to keep the system temperature constant, and then S_{env} can be expressed as

$$dS_{\text{env}} = -\frac{d\_Q}{T}. \tag{2.9}$$

We denote by U the internal energy of the mixture. We assume that the phase equilibrium problem is a sharp interface problem; that is, the interface between two phases has zero width. The internal energy U of the system is viewed as a sum of internal energies of two phases. The first law of thermodynamics states

$$\frac{dU}{dt} = \frac{d\_Q}{dt} + \frac{dW}{dt}. \tag{2.10}$$

Applying the relation between Helmholtz free energy and internal energy of a system $U = F + TS_{\text{sys}}$ to (2.10), and taking into account (2.8), we obtain the heat transfer

$$\frac{d\_Q}{dt} = \frac{dF}{dt} + T\frac{dS_{\text{sys}}}{dt} + p_c\frac{dV^G}{dt}. \tag{2.11}$$

The change of entropy can be derived through (2.9) and (2.11) as

$$\begin{aligned}\frac{dS}{dt} &= \frac{dS_{\text{sys}}}{dt} + \frac{dS_{\text{env}}}{dt}\\ &= \frac{dS_{\text{sys}}}{dt} - \frac{1}{T}\frac{d\_Q}{dt}\\ &= -\frac{1}{T}\frac{dF}{dt} - \frac{p_c}{T}\frac{dV^G}{dt}.\end{aligned} \tag{2.12}$$

We note that there exists another approach to account for the effect of interfacial tension in the literature, for example [6]. In the approach [6], the work contributed by the interfacial or surface tension instead of capillary force is taken into account, and

under the assumption that the gas bubble has a spherical shape, then the interfacial area is related to the gas volume and consequently, the Young-Laplace equation is derived. In this work, we use the approach involving the capillary pressure directly, which is convenient to apply various formulations of the capillary pressure beside the Young-Laplace equation; for example, we can also use the Tolman length [2], which improves the Young-Laplace equation.

We now derive the form of $\frac{dF}{dt}$. The partial derivatives of $F(\mathbf{N}^G, V^G)$ are calculated as

$$\frac{\partial F(\mathbf{N}^G, V^G)}{\partial N_i^G} = \mu_i\left(\mathbf{n}^G\right) - \mu_i\left(\mathbf{n}^L\right), \tag{2.13}$$

$$\frac{\partial F(\mathbf{N}^G, V^G)}{\partial V^G} = p_L - p_G, \tag{2.14}$$

where μ_i is the chemical potential of component i, and $p_L = p(\mathbf{n}^L)$ and $p_G = p(\mathbf{n}^G)$ are the liquid and gas pressures respectively. The use of chain rule yields

$$\begin{aligned}\frac{dF}{dt} &= \frac{\partial F}{\partial V^G}\frac{\partial V^G}{\partial t} + \sum_{i=1}^{M}\frac{\partial F}{\partial N_i^G}\frac{\partial N_i^G}{\partial t} \\ &= \left(p_L - p_G\right)\frac{\partial V^G}{\partial t} + \sum_{i=1}^{M}\left(\mu_i\left(\mathbf{n}^G\right) - \mu_i\left(\mathbf{n}^L\right)\right)\frac{\partial N_i^G}{\partial t}.\end{aligned} \tag{2.15}$$

Substituting (2.15) into (2.12) leads to the change of entropy

$$\frac{dS}{dt} = \frac{1}{T}\left(p_G - p_L - p_c\right)\frac{\partial V^G}{\partial t} + \frac{1}{T}\sum_{i=1}^{M}\left(\mu_i\left(\mathbf{n}^L\right) - \mu_i\left(\mathbf{n}^G\right)\right)\frac{\partial N_i^G}{\partial t}. \tag{2.16}$$

According to Onsager's reciprocal principle [7], there exists a symmetrical matrix $\mathbf{\Psi} = (\psi_{i,j})_{i,j=1}^{M+1}$ such that

$$\frac{\partial N_i^G}{\partial t} = \sum_{j=1}^{M}\psi_{i,j}\left(\mu_j\left(\mathbf{n}^L\right) - \mu_j\left(\mathbf{n}^G\right)\right) + \psi_{i,M+1}\left(p_G - p_L - p_c\right),\ 1 \le i \le M, \tag{2.17}$$

$$\frac{\partial V^G}{\partial t} = \sum_{j=1}^{M}\psi_{M+1,j}\left(\mu_j\left(\mathbf{n}^L\right) - \mu_j\left(\mathbf{n}^G\right)\right) + \psi_{M+1,M+1}\left(p_G - p_L - p_c\right). \tag{2.18}$$

According to the second law of thermodynamics, the total entropy S shall not decrease with time, so $\mathbf{\Psi}$ shall be positive definite.

A simple choice of $\mathbf{\Psi}$ is to take a diagonal positive definite matrix for $\mathbf{\Psi}$ as

$$\psi_{i,i} = \frac{D_i N_i^t}{RT}, \quad i = 1, \cdots, M, \quad \psi_{M+1,M+1} = \frac{C_V^G C_V^L V^t}{C_V^L p_G + C_V^G p_L}, \tag{2.19}$$

where D_i is the diffusion coefficient of component i and C_V^G and C_V^L are the nonzero parameters chosen such that

$$C_V^G p_G \ge 0, \quad C_V^L p_L \ge 0. \tag{2.20}$$

Since the pressures may be negative in NVT flash [8], the above choice of C_V^G and C_V^L can ensure $\psi_{M+1,M+1} > 0$. In this case, we obtain the evolutionary equation for moles of component i as

$$\frac{\partial N_i^G}{\partial t} = \frac{D_i N_i^t}{RT}\left(\mu_i\left(\mathbf{n}^L\right) - \mu_i\left(\mathbf{n}^G\right)\right), \quad i = 1, \cdots, M. \tag{2.21}$$

and the volume evolutionary equation as

$$\frac{\partial V^G}{\partial t} = \frac{C_V^G C_V^L V^t}{C_V^L p_G + C_V^G p_L}\left(p_G - p_L - p_c\right). \tag{2.22}$$

We note that if capillarity effect is ignored, the equations (2.21) and (2.22) can be reduced into the formulations in [14] for NVT flash.

The system composed of the equations (2.21) and (2.22) describes the dynamical process from an initial state (non-equilibrium state) to an equilibrium state in the presence of capillarity effect at the fixed moles, volume and temperature. For NPT-based phase equilibrium model, only temperature or pressure can be specified for a pure substance, while both are usually required to be specified for multi-component mixtures. The specified thermodynamical variables are unified (always N,V and T) for both a pure substance and a multi-component mixture. The initial conditions can be provided by the phase stability analysis, which will be discussed subsequently in Section 4.

We now consider the equilibrium state. Substituting (2.21) and (2.22) into (2.16) yields

$$\frac{dS}{dt} = \frac{1}{T}\frac{C_V^G C_V^L V^t}{C_V^L p_G + C_V^G p_L}\left(p_G - p_L - p_c\right)^2 + \sum_{i=1}^{M}\frac{D_i N_i^t}{RT^2}\left(\mu_i\left(\mathbf{n}^L\right) - \mu_i\left(\mathbf{n}^G\right)\right)^2 \tag{2.23}$$

At the equilibrium state, the entropy attains the maximum value and the state does not change, i.e. $\frac{dS}{dt}$, $\frac{\partial N_i^G}{\partial t}$ and $\frac{\partial V^G}{\partial t}$ are all equal to zero. Consequently, the following equations at the equilibrium state are derived from (2.23) as

$$\mu_i\left(\mathbf{n}^L\right) - \mu_i\left(\mathbf{n}^G\right) = 0, \tag{2.24}$$

$$p_G - p_L - p_c = 0, \tag{2.25}$$

which hold for both a pure substance and a multi-component mixture.

3. Thermodynamically stable numerical method. In this section, we will design the efficient time discretization of the proposed dynamical model given in (2.21) and (2.22). As shown in the previous section, the entropy production is an essential property in the evolutionary process to the equilibrium state. So the numerical methods to preserve this property is preferable. A key ingredient of constructing such methods is the convex splitting of Helmholtz free energy, which will be studied in Subsection 3.1. The numerical scheme will be proposed in Subsection 3.2. We show in Subsection 3.3 that the proposed method is thermodynamically stable.

3.1. Convex splitting of Helmholtz free energy. Entropy stability implies that the total Helmholtz free energy is dissipated with time [15]. It is well-known that both of fully explicit and implicit Euler's method fail to preserve the energy dissipation

unless the time step size is restricted to be sufficiently small [15, 24, 29]. So a semi-implicit scheme is a preferable choice to preserve the entropy stability and admit reasonable large time steps. The effectiveness of convex-concave splitting techniques has been demonstrated in numerical simulation of the realistic fluids [5, 15, 24, 29]. In Subsection 3.3 , we can prove that the convex-concave splitting of Helmholtz free energy density can result in the entropy stability of numerical schemes.

For the pure substance, it was shown in [29] that the Helmholtz free energy density can be split into convex and concave parts. For the multi-component mixture, we use the additional ideal term [15] to construct a strict convex-concave splitting. The Helmholtz free energy density is reformulated as a sum of two parts: one is the convex function denoted by f^{convex}; the other is the concave function denoted by f^{concave}, i.e.

$$f(\mathbf{n}) = f^{\text{convex}}(\mathbf{n}) + f^{\text{concave}}(\mathbf{n}), \tag{3.1}$$

$$f^{\text{convex}}(\mathbf{n}) = (1+\lambda)\, f^{\text{ideal}}(\mathbf{n}) + f^{\text{repulsion}}(\mathbf{n}), \tag{3.2}$$

$$f^{\text{concave}}(\mathbf{n}) = f^{\text{attraction}}(\mathbf{n}) - \lambda f^{\text{ideal}}(\mathbf{n}), \tag{3.3}$$

where $\lambda \geq 0$. Correspondingly, the chemical potential can be expressed a sum of two parts as

$$\mu_i(\mathbf{n}) = \mu_i^{\text{convex}}(\mathbf{n}) + \mu_i^{\text{concave}}(\mathbf{n}), \tag{3.4}$$

where

$$\mu_i^{\text{convex}} = \left(\frac{\partial f^{\text{convex}}}{\partial n_i}\right)_{T,n_j,j\neq i}, \quad \mu_i^{\text{concave}} = \left(\frac{\partial f^{\text{concave}}}{\partial n_i}\right)_{T,n_j,j\neq i}.$$

It has been shown in [15] that there exist suitable values of λ to gain the strict convex-concave splitting for the Helmholtz free energy density. In practical computations, the values of λ are suggested between 0.1 and 10.

Based on the above convex-concave splitting of Helmholtz free energy density, we can split the total Helmholtz free energy F, which is a function of $\mathbf{N}^G$ and V^G, into the following form

$$F(\mathbf{N}^G, V^G) = F_c(\mathbf{N}^G, V^G) + F_a(\mathbf{N}^G, V^G), \tag{3.5}$$

where

$$F_c(\mathbf{N}^G, V^G) = f^{\text{convex}}(\mathbf{n}^G)V^G + f^{\text{convex}}(\mathbf{n}^L)V^L, \tag{3.6}$$

$$F_a(\mathbf{N}^G, V^G) = f^{\text{concave}}(\mathbf{n}^G)V^G + f^{\text{concave}}(\mathbf{n}^L)V^L. \tag{3.7}$$

We now analyze the convex-concave properties of F_c and F_a. The second-order partial derivatives of F_c with respect to N_i^G and N_j^G are calculated as

$$\frac{\partial^2 F_c(\mathbf{N}^G, V^G)}{\partial N_i^G \partial N_j^G} = \frac{\partial^2 f^{\text{convex}}\left(\mathbf{n}^G\right)}{\partial n_i^G \partial n_j^G}\frac{1}{V^G} + \frac{\partial^2 f^{\text{convex}}\left(\mathbf{n}^L\right)}{\partial n_i^L \partial n_j^L}\frac{1}{V^L}. \tag{3.8}$$

Owing to the convexity of f^{convex}, using the features of the positive definite matrix, we can conclude from (3.8) that F_c is convex with respect to $\mathbf{N}^G$. Moreover, F_c is also convex with respect to V^G on account of the second-order partial derivative of F_c with respect to V^G

$$\frac{\partial^2 F_c(\mathbf{N}^G, V^G)}{\partial V^G \partial V^G} = \sum_{i,j=1}^{M} \frac{\partial^2 f^{\text{convex}}\left(\mathbf{n}^G\right)}{\partial n_i^G \partial n_j^G} \frac{n_i^G n_j^G}{V^G} + \sum_{i,j=1}^{M} \frac{\partial^2 f^{\text{convex}}\left(\mathbf{n}^L\right)}{\partial n_i^L \partial n_j^L} \frac{n_i^L n_j^L}{V^L}. \quad (3.9)$$

Applying the similar analysis approaches to F_a, we can derive that F_a is concave with respect to $\mathbf{N}^G$ or V^G.

3.2. Semi-implicit numerical scheme. We now present a thermodynamically stable semi-implicit time-matching method. The mass conservation equations (in moles) and the volume equation will be solved separately by the mixed explicit-implicit schemes.

The total time interval is chosen as $I = (0, T_f]$, where $T_f > 0$. We divide I into K subintervals $I_k = (t_k, t_{k+1}]$, where $t_0 = 0$ and $t_K = T_f$. The time step size is denoted by $\delta t_k = t_{k+1} - t_k$. We denote by $\mathbf{N}^{G,k}$ and $\mathbf{N}^{L,k}$ the approximate gas and liquid moles at the kth time step, and denote by $V^{G,k}$ and $V^{L,k}$ the approximate gas and liquid volumes at the kth time step.

The molar densities at the kth time step are calculated as $\mathbf{n}^{G,k} = \frac{\mathbf{N}^{G,k}}{V^{G,k}}$ and $\mathbf{n}^{L,k} = \frac{\mathbf{N}^{L,k}}{V^{L,k}}$. Furthermore, the notations of $\mathbf{n}^{G,k+\frac{1}{2}}$ and $\mathbf{n}^{L,k+\frac{1}{2}}$ are used to represent

$$\mathbf{n}^{G,k+\frac{1}{2}} = \frac{\mathbf{N}^{G,k+1}}{V^{G,k}}, \quad \mathbf{n}^{L,k+\frac{1}{2}} = \frac{\mathbf{N}^{L,k+1}}{V^{L,k}}.$$

The temporal discrete equation for moles of component i $(i = 1, \cdots, M)$ is expressed as

$$\frac{N_i^{G,k+1} - N_i^{G,k}}{\delta t_k} = \frac{D_i N_i^t}{RT} \left(\mu_i^{L,k+\frac{1}{2}} - \mu_i^{G,k+\frac{1}{2}}\right), \quad (3.10)$$

where

$$\mu_i^{G,k+\frac{1}{2}} = \mu_i^{\text{convex}}\left(\mathbf{n}^{G,k+\frac{1}{2}}\right) + \mu_i^{\text{concave}}\left(\mathbf{n}^{G,k}\right),$$

$$\mu_i^{L,k+\frac{1}{2}} = \mu_i^{\text{convex}}\left(\mathbf{n}^{L,k+\frac{1}{2}}\right) + \mu_i^{\text{concave}}\left(\mathbf{n}^{L,k}\right).$$

The equations (3.10) lead to a nonlinear system, unknowns of which are the gas-phase moles of all components $\mathbf{N}^{G,k+1}$ at the $(k+1)$th time step. But this system is independent of the gas volume $V^{G,k+1}$ at the $(k+1)$th time step. Once $\mathbf{N}^{G,k+1}$ is computed, we use the following discrete volume evolutionary equation to calculate the gas volume at the $(k+1)$th time step as

$$\frac{V^{G,k+1} - V^{G,k}}{\delta t_k} = \frac{C_V^G C_V^L V^t}{C_V^L p_G^k + C_V^G p_L^k} \left(p_G^{k+\frac{1}{2}} - p_L^{k+\frac{1}{2}} - p_c^{k+\frac{1}{2}}\right), \quad (3.11)$$

where

$$p_G^{k+\frac{1}{2}} = \sum_{j=1}^{M} \left(n_j^{G,k+1} \mu_j^{\text{convex}}\left(\mathbf{n}^{G,k+1}\right) + n_j^{G,k+\frac{1}{2}} \mu_j^{\text{concave}}\left(\mathbf{n}^{G,k+\frac{1}{2}}\right)\right)$$

$$-f^{\text{convex}}(\mathbf{n}^{G,k+1}) + f^{\text{concave}}(\mathbf{n}^{G,k+\frac{1}{2}}), \tag{3.12}$$

$$p_L^{k+\frac{1}{2}} = \sum_{j=1}^{M} \left(n_j^{L,k+1} \mu_j^{\text{convex}} \left(\mathbf{n}^{L,k+1} \right) + n_j^{L,k+\frac{1}{2}} \mu_j^{\text{concave}} \left(\mathbf{n}^{L,k+\frac{1}{2}} \right) \right) - f^{\text{convex}}(\mathbf{n}^{L,k+1}) + f^{\text{concave}}(\mathbf{n}^{L,k+\frac{1}{2}}), \tag{3.13}$$

$$p_c^{k+\frac{1}{2}} = p_c \left(\mathbf{N}^{G,k+1}, V^{G,k} \right). \tag{3.14}$$

Here, $\mathbf{n}^{G,k+1} = \frac{\mathbf{N}^{G,k+1}}{V^{G,k+1}}$ and $\mathbf{n}^{L,k+1} = \frac{\mathbf{N}^{L,k+1}}{V^{L,k+1}} = \frac{\mathbf{N}^t - \mathbf{N}^{G,k+1}}{V^t - V^{L,k+1}}$, so (3.11) is an equation regarding the gas volume $V^{G,k+1}$ only.

3.3. Thermodynamical stability of the numerical scheme. We first introduce the definition of thermodynamical stability, which is desired by an efficient scheme. According to the second law of thermodynamics, the total entropy increases over time, i.e. $\frac{dS}{dt} \geq 0$, and thereby it is derived from (2.12) that

$$\frac{dF}{dt} + p_c \frac{dV^G}{dt} \leq 0. \tag{3.15}$$

Integrating (3.15) over the time interval $(t_k, t_{k+1}]$ gives

$$F^{k+1} - F^k + \int_{t_k}^{t_{k+1}} p_c \frac{\partial V^G}{\partial t} \leq 0, \tag{3.16}$$

where $F^k = F(\mathbf{N}^{G,k}, V^{G,k})$. If p_c is a given constant, then the inequality (3.16) is reduced into

$$F^{k+1} - F^k + p_c \left(V^{G,k+1} - V^{G,k} \right) \leq 0. \tag{3.17}$$

If p_c is a function of $\mathbf{N}^G$ and V^G, then we apply the quadrature rule to (3.16) and get

$$F^{k+1} - F^k + p_c^\star \left(V^{G,k+1} - V^{G,k} \right) \leq 0, \tag{3.18}$$

where $p_c^\star$ is a capillary pressure value between kth and $(k+1)$th time steps. For a specific discretization of capillary pressure, if a discrete scheme satisfies the inequality of the type in (3.17) or (3.18), then we call this scheme as a thermodynamically stable scheme. If capillarity is neglected, then the thermodynamical stability becomes the energy stability.

We now analyze the thermodynamical stability of the proposed method. Multiplying (3.10) by $\left(\mu_i^{G,k+\frac{1}{2}} - \mu_i^{L,k+\frac{1}{2}} \right)$

$$\left(\mu_i^{G,k+\frac{1}{2}} - \mu_i^{L,k+\frac{1}{2}} \right) \frac{N_i^{G,k+1} - N_i^{G,k}}{\delta t_k} = -\frac{D_i N_i^t}{RT} \left(\mu_i^{L,k+\frac{1}{2}} - \mu_i^{G,k+\frac{1}{2}} \right)^2. \tag{3.19}$$

Summing (3.19) from $i = 1$ to M and taking into account the convex-concave property, we obtain

$$\frac{F(\mathbf{N}^{G,k+1}, V^{G,k}) - F(\mathbf{N}^{G,k}, V^{G,k})}{\delta t_k} \leq -\sum_{i=1}^{M} \frac{D_i N_i^t}{RT} \left(\mu_i^{L,k+\frac{1}{2}} - \mu_i^{G,k+\frac{1}{2}} \right)^2. \tag{3.20}$$

We multiply (3.11) by $\left(p_L^{k+\frac{1}{2}} - p_G^{k+\frac{1}{2}} + p_c^{k+\frac{1}{2}}\right)$ and derive

$$\left(p_L^{k+\frac{1}{2}} - p_G^{k+\frac{1}{2}} + p_c^{k+\frac{1}{2}}\right) \frac{V^{G,k+1} - V^{G,k}}{\delta t_k} = -\frac{C_V^G C_V^L V^t}{C_V^L p_G^k + C_V^G p_L^k} \left(p_G^{k+\frac{1}{2}} - p_L^{k+\frac{1}{2}} - p_c^{k+\frac{1}{2}}\right)^2. \tag{3.21}$$

Through the convex-concave property of F with respect to the gas volume, we get

$$F(\mathbf{N}^{G,k+1}, V^{G,k+1}) - F(\mathbf{N}^{G,k+1}, V^{G,k}) \leq \left(p_L^{k+\frac{1}{2}} - p_G^{k+\frac{1}{2}}\right) \left(V^{G,k+1} - V^{G,k}\right). \tag{3.22}$$

We denote $F^k = F(\mathbf{N}^{G,k}, V^{G,k})$ and $F^{k+1} = F(\mathbf{N}^{G,k+1}, V^{G,k+1})$, and then combining (3.20)-(3.22), we derive that

$$\begin{aligned} F^{k+1} - F^k + p_c^{k+\frac{1}{2}} \left(V^{G,k+1} - V^{G,k}\right) &\leq -\frac{D_i N_i^t}{RT} \left(\mu_i^{L,k+\frac{1}{2}} - \mu_i^{G,k+\frac{1}{2}}\right)^2 \\ &\quad - \frac{C_V^G C_V^L V^t}{C_V^L p_G^k + C_V^G p_L^k} \left(p_G^{k+\frac{1}{2}} - p_L^{k+\frac{1}{2}} - p_c^{k+\frac{1}{2}}\right)^2 \\ &\leq 0. \end{aligned} \tag{3.23}$$

As a result of (3.23), the entropy shall increase with time steps even for large time step sizes until it reaches a maximum. When the entropy attains its maximum, the system reaches the equilibrium state. This means that the proposed scheme obeys the second law of thermodynamics, so the proposed scheme has the thermodynamical stability (entropy stability) for any time step size.

4. Phase stability analysis with capillarity and initial conditions. The appropriate initial conditions, including initial values of moles and volumes, are required for the proposed dynamical model. To determine the initial conditions, we need to carry out the phase stability analysis with capillarity. The goal of phase stability is to ascertain whether the fluid system remains in a single phase or splits into more phases at specified moles, volume and temperature under consideration of capillarity effect. In [33], the stability analysis was developed for multicomponent mixtures including capillary pressure at specified pressure, temperature, and chemical composition. In [22], the phase stability analysis without capillarity effect was developed at specified moles, volume and temperature. In this work, we will develop the phase stability analysis with capillarity at specified moles, volume and temperature using the entropy principle.

4.1. Phase stability analysis. We consider the changes of primal thermodynamical variables when a single-phase system splits into two phases. First, the total entropy change, denoted by ΔS, shall be positive as a conclusion of the second law of thermodynamics. Indeed, ΔS contains two contributions as $\Delta S = \Delta S_{\text{sys}} + \Delta S_{\text{env}}$, where the first is the entropy change of the system, and the second is the entropy change of the environment expressed as

$$\Delta S_{\text{env}} = -\frac{\Delta\_Q}{T}. \tag{4.1}$$

Here, Δ_Q is the heat transfer quantity from the environment in order to keep the system temperature constant. Let ΔU be the change of internal energy of the mixture. The work done by the capillary pressure is denoted by ΔW. The first law of

thermodynamics reads as

$$\Delta U = \Delta\_Q + \Delta W. \tag{4.2}$$

Let ΔV^G be the change of the gas-phase volume. We can express $\Delta W = -p_c \Delta V^G$ similarly to (2.8), and then we obtain

$$\Delta\_Q = \Delta F + T\Delta S_{\text{sys}} + p_c \Delta V^G, \tag{4.3}$$

where ΔF is the change of total Helmholtz free energy. The total entropy change can be derived as

$$\Delta S = \Delta S_{\text{sys}} - \frac{1}{T}\Delta\_Q = -\frac{1}{T}\Delta F - \frac{p_c}{T}\Delta V^G. \tag{4.4}$$

If the feed mixture is assumed to be gas, then the trial phase is liquid; in this case, taking $V' = V^L > 0$ and $\mathbf{N}' = \mathbf{N}^L > 0$, we have $\Delta V^G = -V^L$, and using the derivations similar to [22], we can derive the change of total Helmholtz free energy as

$$\begin{aligned}\Delta F &= F\left(V^L, T, \mathbf{N}^L\right) + F\left(V^t - V^L, T, \mathbf{N}^t - \mathbf{N}^L\right) - F\left(V^t, T, \mathbf{N}^t\right) \\ &= \sum_{i=1}^{M}\left(\mu_i\left(V^L, T, \mathbf{N}^L\right) - \mu_i\left(V^t, T, \mathbf{N}^t\right)\right) N_i^L \\ &\quad - \left(p\left(V^L, T, \mathbf{N}^L\right) - p\left(V^t, T, \mathbf{N}^t\right)\right) V^L + R_1\left(V^L, T, \mathbf{N}^L\right),\end{aligned} \tag{4.5}$$

where the pressure (p) and chemical potentials (μ_i) are treated as functions of volume, temperature and moles, and R_1 represents the reminder in the Taylor's expansion after the first-order terms.

If the feed mixture is assumed to be liquid, then the trial phase is gas. In this case, we take $V' = V^G > 0$, $\mathbf{N}' = \mathbf{N}^G > 0$, and then $\Delta V^G = V^G$. The change of total Helmholtz free energy is similarly derived as

$$\begin{aligned}\Delta F &= \sum_{i=1}^{M}\left(\mu_i\left(V^G, T, \mathbf{N}^G\right) - \mu_i\left(V^t, T, \mathbf{N}^t\right)\right) N_i^G \\ &\quad - \left(p\left(V^G, T, \mathbf{N}^G\right) - p\left(V^t, T, \mathbf{N}^t\right)\right) V^G + R_1\left(V^G, T, \mathbf{N}^G\right).\end{aligned} \tag{4.6}$$

For sufficiently small perturbations $(V', T, \mathbf{N}')$, combining (4.4) with (4.5) and (4.6), we obtain

$$\begin{aligned}-T\Delta S &= \Delta F + p_c \Delta V^G \\ &= \sum_{i=1}^{M}\left(\mu_i\left(V', T, \mathbf{N}'\right) - \mu_i\left(V^t, T, \mathbf{N}^t\right)\right) N_i' \\ &\quad - \left(p\left(V', T, \mathbf{N}'\right) - p\left(V^t, T, \mathbf{N}^t\right)\right) V' + \gamma_s p_c V' + R_1\left(V', T, \mathbf{N}'\right).\end{aligned} \tag{4.7}$$

In (4.7), if the feed mixture is assumed to be liquid and the trial phase is gas, then we take $\gamma_s = 1$; otherwise, that is, the feed mixture is gas and the trial phase is liquid, then we take $\gamma_s = -1$.

The single phase is stable if $\Delta S \leq 0$ according to the second law of thermodynamics. We assume that the remainder term $R_1\left(V', T, \mathbf{N}'\right)$ cannot change the sign of $(-T\Delta S)$, and from this, we conclude that the single phase is stable if

$$\sum_{i=1}^{M}\left(\mu_i\left(V', T, \mathbf{N}'\right) - \mu_i\left(V^t, T, \mathbf{N}^t\right)\right) N_i'$$

$$-\left(p\left(V',T,\mathbf{N}'\right)-p\left(V^t,T,\mathbf{N}^t\right)\right)V'+\gamma_s p_c V'\geq 0. \tag{4.8}$$

We now rewrite (4.8) into a more convenient form. We denote the overall molar density $\mathbf{n}^t=\frac{\mathbf{N}^t}{V^t}$ and the trial phase molar density $\mathbf{n}'=\frac{\mathbf{N}'}{V'}$. We note that the pressure and chemical potentials are homogeneous functions of degree zero with respect to volume and moles, so they can also be viewed as functions of molar densities and temperature. Dividing (4.8) by V', we define the tangent plane distance function as

$$\Psi(\mathbf{n}',T)=\sum_{i=1}^{M}n_i'\left(\mu_i\left(T,\mathbf{n}'\right)-\mu_i\left(T,\mathbf{n}^t\right)\right)-\left(p\left(T,\mathbf{n}'\right)-p\left(T,\mathbf{n}^t\right)\right)+\gamma_s p_c, \tag{4.9}$$

where p_c depends on $\mathbf{n}'$ and $\mathbf{n}^t$. If capillarity is neglected, i.e. $p_c=0$, (4.9) is reduced into the form proposed in [22]. The single phase is stable if and only if $\Psi(\mathbf{n}',T)\geq 0$ holds for all admissible molar density $\mathbf{n}'$ at the temperature T.

We will rewrite (4.9) into another form. Using the relation $p=\sum_{i=1}^{M}n_i\mu_i-f$, we introduce a function of molar density $\mathbf{n}$ and temperature T as

$$\Phi(\mathbf{n},T)=f\left(\mathbf{n},T\right)-\sum_{i=1}^{M}n_i\mu_i\left(\mathbf{n}^t,T\right). \tag{4.10}$$

Thus, the tangent plane distance function can be reformulated as

$$\Psi(\mathbf{n}',T)=\Phi(\mathbf{n}',T)-\Phi(\mathbf{n}^t,T)+\gamma_s p_c. \tag{4.11}$$

The single-phase is stable if and only if Ψ has a nonnegative minimum. The minimizer $\mathbf{n}^*$ of Ψ at temperature T shall satisfy

$$\mu_i\left(\mathbf{n}^*\right)-\mu_i\left(\mathbf{n}^t\right)+\gamma_s\frac{\partial p_c(\mathbf{n}^*)}{\partial n_i}=0,\quad i=1,\cdots,M. \tag{4.12}$$

4.2. Numerical method. In order to find $\mathbf{n}^*$, we use the following evolution equation for the molar density of component i as

$$\frac{\partial n_i}{\partial t}=-\frac{D_i n_i^t}{RT}\left(\mu_i\left(\mathbf{n}\right)-\mu_i\left(\mathbf{n}^t\right)+\gamma_s\frac{\partial p_c(\mathbf{n})}{\partial n_i}\right),\quad i=1,\cdots,M. \tag{4.13}$$

Multiplying both sides of (4.13) by $\left(\mu_i\left(\mathbf{n}\right)-\mu_i\left(\mathbf{n}^t\right)+\gamma_s\frac{\partial p_c(\mathbf{n})}{\partial n_i}\right)$ and then summing it from 1 to M, we can obtain that the system given by (4.13) satisfies the dissipation property

$$\frac{\partial\Psi}{\partial t}=-\sum_{i=1}^{M}\frac{D_i n_i^t}{RT}\left(\mu_i\left(\mathbf{n}\right)-\mu_i\left(\mathbf{n}^t\right)+\gamma_s\frac{\partial p_c(\mathbf{n})}{\partial n_i}\right)^2, \tag{4.14}$$

which means that the minimizer of Ψ can be achieved after an evolutionary period.

Applying the convex-concave splitting of $f(\mathbf{n})$, we construct a semi-implicit time scheme for time discretization of (4.13) as

$$\frac{n_i^{k+1}-n_i^k}{\delta t_k}=-\frac{D_i n_i^t}{RT}\left(\mu_i^{\text{convex}}\left(\mathbf{n}^{k+1}\right)+\mu_i^{\text{concave}}\left(\mathbf{n}^k\right)-\mu_i\left(\mathbf{n}^t\right)+\gamma_s\frac{\partial p_c(\mathbf{n}_*^k)}{\partial n_i}\right) \tag{4.15}$$

where $i=1,\cdots,M$. In (4.15), $\frac{\partial p_c(\mathbf{n}_*^k)}{\partial n_i}$ vanishes for the case that p_c is independent of $\mathbf{n}$; otherwise, $\mathbf{n}_*^k$ is determined by the value of γ_s and convexity/concavity of p_c. When

we use the Young-Laplace equation and Weinaug–Katz correlation [39] to calculate p_c, $\mathbf{n}_*^k$ is taken as

$$\mathbf{n}_*^k = \begin{cases} \mathbf{n}^{k+1}, \ \gamma_s = 1, \\ \mathbf{n}^k, \ \ \gamma_s = -1. \end{cases} \tag{4.16}$$

The discrete scheme given by (4.15) preserves the following key stability feature

$$\Psi(\mathbf{n}^{k+1}) \leq \Psi(\mathbf{n}^k). \tag{4.17}$$

Indeed, applying the convex-concave properties, we obtain

$$\frac{\Psi(\mathbf{n}^{k+1}) - \Psi(\mathbf{n}^k)}{\delta t_k} \leq -\sum_{i=1}^{M} \frac{D_i n_i^t}{RT} \left(\mu_i^{\text{convex}} \left(\mathbf{n}^{k+1}\right) + \mu_i^{\text{concave}} \left(\mathbf{n}^k\right) - \mu_i \left(\mathbf{n}^t\right) + \gamma_s \frac{\partial p_c(\mathbf{n}_*^k)}{\partial n_i} \right)^2,$$

which leads to (4.17). The feature (4.17) ensures that a minimum point of Ψ can be reached after a certain amount of time steps.

The numerical scheme (4.15) of phase stability testing still requires an initial composition $\mathbf{n}^0$, which is taken through a strategy suggested in [22]. This strategy can provide at most four feasible compositions as the initial molar density of one phase. The details of choosing $\mathbf{n}^0$ can be found in [22]. We now describe how to choose the initial conditions for the NVT-flash calculation presented in the Subsection 3.2. If $\Psi \geq 0$ is satisfied for all solutions of phase stability testing, the system is in a single phase and the NVT-flash calculation is avoided. If there exists a trial molar density $\mathbf{n}'$ such that $\Psi(\mathbf{n}', T) < 0$, then the system splits into phases. From the derivation of (4.8), we know that (4.8) is an approximation of $\Delta F + p_c \Delta V^G$ as ΔV^G is sufficiently small. We can use the bisection method to find a small volume $V' > 0$ such that

$$F\left(V', T, \mathbf{N}'\right) + F\left(V^t - V', T, \mathbf{N}^t - \mathbf{N}'\right) - F\left(V^t, T, \mathbf{N}^t\right) + \gamma_s p_c V' < 0, \tag{4.18}$$

where $\mathbf{N}' = \mathbf{n}' V'$ and p_c is calculated from $\mathbf{n}'$ and $\mathbf{n}^t$ if it depends on molar densities. We use the method of selecting a reference component [23] to specify the phase identification, which is based on the fact that the reference component has the larger molar density in the liquid phase than in the gas phase. In (4.18), we can easily know that $\gamma_s = 1$ if $n_r' < n_r^t$, and $\gamma_s = -1$ if $n_r' > n_r^t$, where the subscript r represents the reference component. Once V' satisfying (4.18) is obtained, we can get the initial conditions for the NVT-flash calculation presented in the Subsection 3.2 as following

$$\mathbf{N}^{G,0} = \mathbf{n}' V', \ \ V^{G,0} = V', \ \ \text{if } \gamma_s = 1, \tag{4.19}$$

$$\mathbf{N}^{G,0} = \mathbf{N}^t - \mathbf{n}' V', \ \ V^{G,0} = V^t - V', \ \ \text{if } \gamma_s = -1. \tag{4.20}$$

5. Numerical tests. In this section, we carry out various numerical tests on a pure substance and a binary mixture. We first summarize the computational algorithms.

First, the phase stability testing is carried out to provide the initial conditions. For the time scheme (4.15), we take the time step size $\Delta t_k = 10$, and we set the number of total time steps is 200. Moreover, we terminate the time step loop if $\|\mathbf{n}^{k+1} - \mathbf{n}^k\|_2 < 1e-5$. The nonlinear system of equations given by (4.15) is solved by Newton's method, and the number of total Newton's iterations is set equal to 10.

We also use the stop criterion that the Euclidian norm of the equation residuals is less than $1e-5$.

Second, we solve the equations (3.10) and (3.11) to get the mole numbers and volume of gas phase at the $(k+1)$th time step. The time step size is set as $\Delta t_k = 10^8$, and the number of total time steps is 1000. We denote $\boldsymbol{\mu} = [\mu_1, \cdots, \mu_M]^T$, and further define the relative errors as

$$\|\Delta \boldsymbol{\mu}^k\|_{rel} = \frac{\|\boldsymbol{\mu}\left(\mathbf{n}^{L,k}\right) - \boldsymbol{\mu}\left(\mathbf{n}^{G,k}\right)\|_2}{\max\left(\|\boldsymbol{\mu}\left(\mathbf{n}^{L,k}\right)\|_2, \|\boldsymbol{\mu}\left(\mathbf{n}^{G,k}\right)\|_2\right)},$$

$$|\Delta p^k|_{rel} = \frac{|p_G^k - p_L^k - p_c^k|}{\max\left(|p_G^k|, |p_L^k|\right)}.$$

The convergence criterion of the time loops is $\max\left(\|\Delta \boldsymbol{\mu}^k\|_{rel}, |\Delta p^k|_{rel}\right) < 1e-3$. Newton's method is used to solve the equations (3.10) and (3.11). The number of total Newton's iterations is set equal to 10, and the stop criterion of Newton's iterations is that the Euclidian norm of the equation residuals is less than $1e-5$.

We now discuss the selection of parameters in the dynamical model. D_i is the diffusion coefficient of component i, so it shall be positive. The choices of C_V^G and C_V^L shall satisfy the condition (2.20) to ensure the positivity of $\psi_{M+1,M+1}$ in (2.19) when a phase pressure is negative. In numerical tests, we find that it is better that the parameters have the same order in quantity, so we select the parameters as $D_i = 1$ and $|C_V^G| = |C_V^L| = 1$. In numerical tests, we take the overall volume being equal to 1m^3. We choose $\lambda = 0.1$ in (3.2) and (3.3). The physical parameters used in numerical tests are listed in Tables 5.1 and 5.2.

Table 5.1: Component physical parameters

Component	Critical pressure(bar)	Critical temperature(K)	Acentric factor
methane	45.99	190.56	0.011
butane	38	424.9	0.193
pentane	33.70	469.7	0.251

Table 5.2: Component parachors

Component	methane	butane	pentane
Parachor($\text{dyne}^{0.25}$ $\text{cm}^{2.75}$/g mol)	77.3	189.9	233.9

5.1. Pure substance: $\mathbf{nC_4}$. In this example, we investigate two-phase equilibria for pure n-butane (nC_4) at various conditions.

We first display the numerical performance of the proposed dynamical method for phase equilibrium calculations. For this purpose, we use a constant surface tension $\sigma = 1$ mN/m, and in this case, the entropy at the $(k+1)$th time step has a simple form as

$$S^{k+1} = S^k - \frac{F^{k+1} - F^k}{T} - \frac{p_c}{T}\left(V^{G,k+1} - V^{G,k}\right), \tag{5.1}$$

where $p_c = \frac{2\sigma\cos\theta}{r}$. We simulate the phase equilibria of nC_4 with two different overall molar densities $n = 1$ kmol/m^3 and $n = 3$ kmol/m^3 at the conditions $r = 10$ nm,

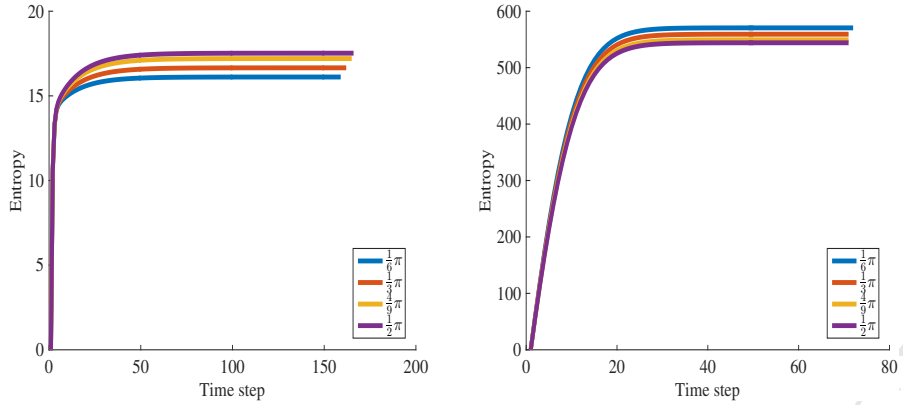

(a) $n = 1$ kmol/m^3 (b) $n = 3$ kmol/m^3

Fig. 5.1: Entropy profiles of nC_4 with two different overall molar densities $n = 1$ kmol/m^3 and $n = 3$ kmol/m^3.

$T = 360$ K and various contact angles. In Figs. 5.1, we illustrate the results of the relative entropy $(S^k - S^0)$. We note that for provided initial conditions, the work done by capillary pressure in the evolution processes may be positive for the case of gas compression, while it may become negative for the case of gas expansion, so it may lead to different effects on the entropy, which can be observed in Fig. 5.1. We can see that the entropy increases with time steps in each case, and thus, the entropy stability feature of the proposed method is verified.

In order to show the performance of the proposed numerical method (4.15) for phase stability calculations, we simulate the phase stability analysis of nC_4 with two different overall molar densities $n = 1$ kmol/m^3 and $n = 3$ kmol/m^3 at the conditions $r = 10$ nm, $T = 360$ K and various contact angles. In the numerical scheme (4.15), the initial condition is $n^0 = 8504.5$ mol/m^3, which is the one calculated in terms of the strategy proposed in [22]. The tangent plane distance (TPD) profiles are depicted in Fig. 5.2. We can see that the TPD function decreases with time steps in all cases, agreeing with the stability feature (4.17). It is also observed that TPD values decrease due to capillarity effect.

At the specified condition $n = 3$ kmol/m^3, $r = 10$ nm and $\theta = \pi/6$, the state variables at the equilibrium states are viewed as functions of the temperature. The phase density and saturation profiles are illustrated in Figs. 5.3 and 5.4 respectively. For the sake of comparison, we also depict the results without capillary pressure at the same conditions.

Comparing the results in Figs. 5.3, we can see that molar densities of both phases are compressed due to capillarity. Fig. 5.4 show that the liquid saturation increases with the increasing temperature, and moreover, comparing the case without capillary pressure, we can see an increase in the liquid saturation due to capillarity effect at various temperatures, which is in agreement with the results in [36]. As shown in [36], Fig. 5.5(a) depicts that the gas-phase saturation pressure can be reduced by capillarity effect, while Fig. 5.5(b) shows that the capillary pressure becomes weaker as the temperature increases. The variation of gas-phase saturation pressure is in accordance with the Kelvin equation, while the increasing temperature reduces the difference between phase densities and consequently, the capillary pressure decreases.

At the specified condition $T = 360$ K, $r = 10$ nm and $\theta = \pi/6$, the equilibrium

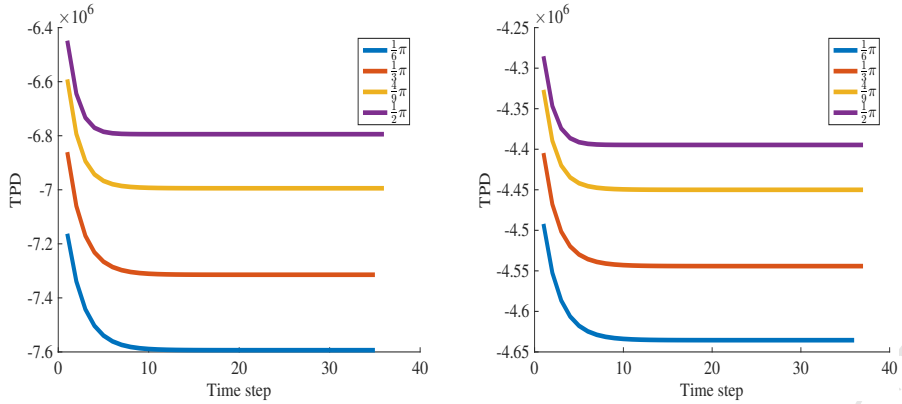

(a) $n = 1$ kmol/m^3 (b) $n = 3$ kmol/m^3

Fig. 5.2: Tangent plane distance (TPD) profiles of nC_4 with two different overall molar densities $n = 1$ kmol/m^3 and $n = 3$ kmol/m^3.

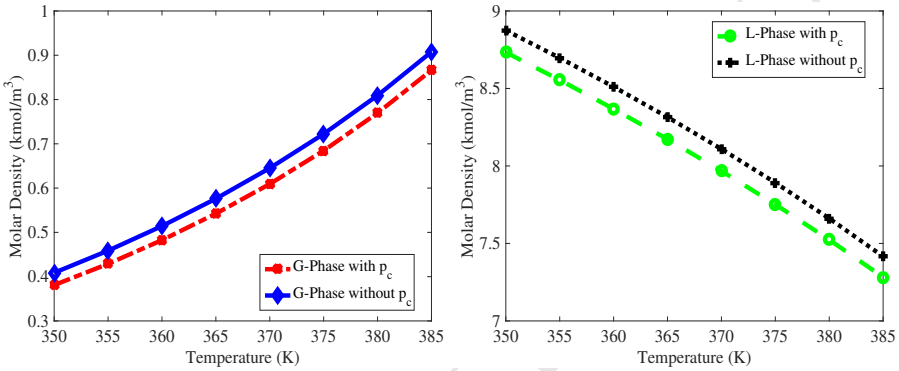

Fig. 5.3: Phase molar densities as functions of the temperature: nC_4 at $n = 3$ kmol/m^3, $r = 10$ nm and $\theta = \pi/6$.

state variables can be viewed as functions of the overall molar density. We show the phase density profiles of nC_4 in Fig. 5.6(a), while the gas saturation profile is shown in Fig. 5.6(b). The phase pressure and capillary pressure profiles are illustrated in Figs. 5.7(a) and 5.7(b).

We calculate the phase equilibria at $n = 3$ kmol/m^3, $T = 360$ K and different contact angles. For specified overall molar density, temperature and contact angle, the equilibrium state variables can be viewed as functions of the pore radius. The saturation pressure profiles are illustrated in Fig. 5.8(a), in which we also illustrate the saturation pressures calculated by the Kelvin equation [6]. The capillary pressure profile is shown in Fig. 5.8(b). The phase density and saturation profiles are illustrated in Figs. 5.9 and 5.10 respectively.

Fig. 5.8(a) indicates that the calculated saturation pressures agree with the Kelvin equation in the envelope of the relationship between the pore radius and saturation pressure at various contact angles. As shown in Fig. 5.8(b), the capillary pressure decreases with the pore radius, which is consistent with Young-Laplace equation. Fig. 5.9 shows that molar densities of both phases increase in proportion to the pore radius and contact angle, and thus, as shown in Fig. 5.10, the liquid volume

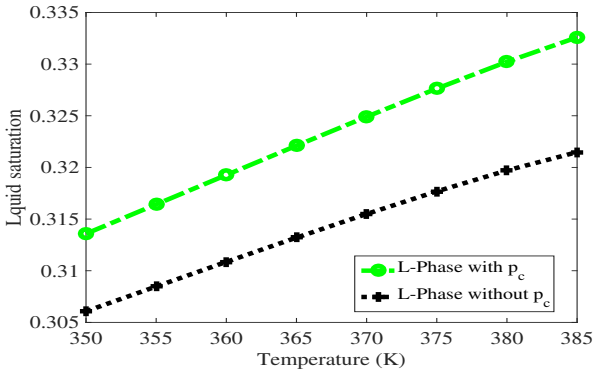

Fig. 5.4: Liquid saturation as a function of the temperature: nC_4 at $n = 3$ kmol/m^3, $r = 10$ nm and $\theta = \pi/6$.

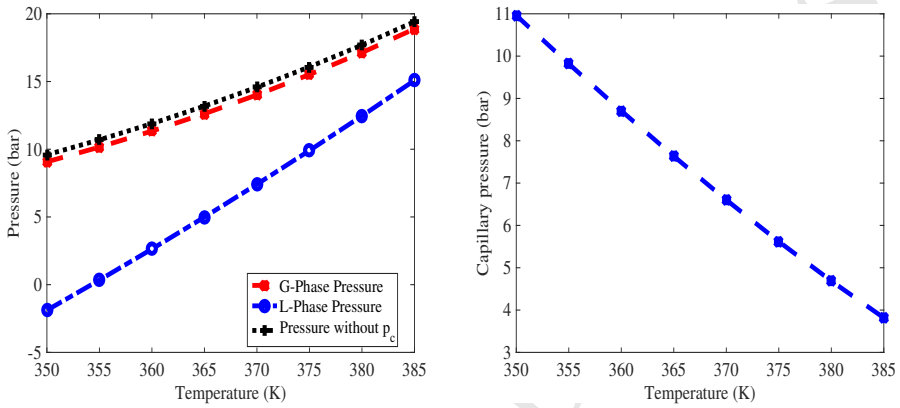

(a) Phase pressure (b) Capillary pressure

Fig. 5.5: Phase pressure and capillary pressure as functions of the temperature: nC_4 at $n = 3$ kmol/m^3, $r = 10$ nm and $\theta = \pi/6$.

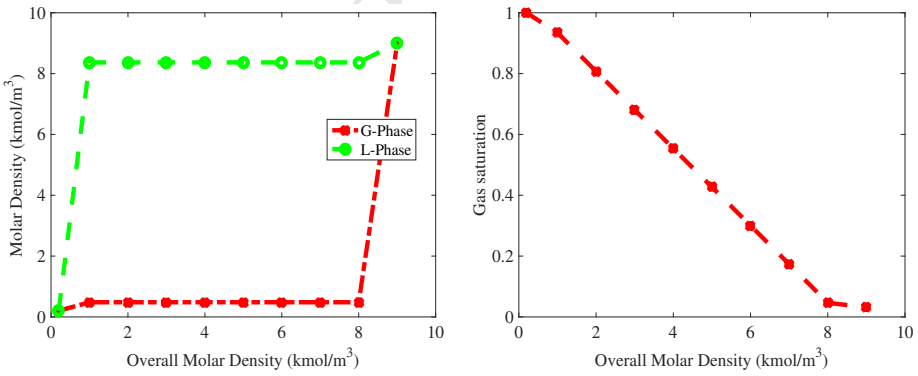

(a) Phase molar density (b) Gas saturation

Fig. 5.6: Phase molar density and gas saturation as functions of the overall molar density: nC_4 at $T = 360$ K, $r = 10$ nm and $\theta = \pi/6$.

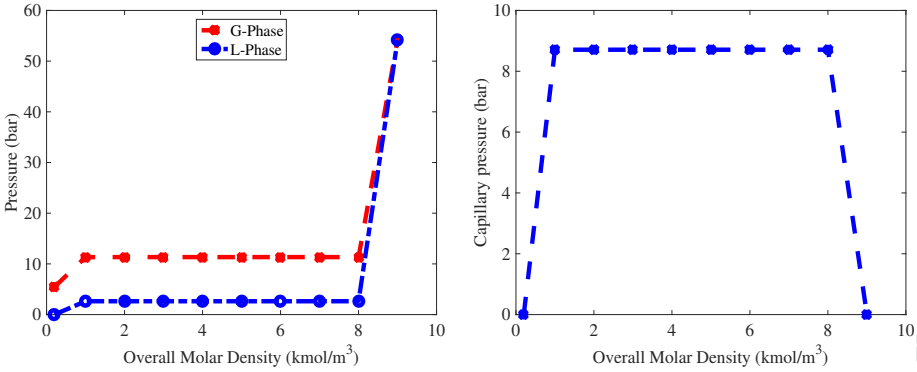

(a) Phase pressure (b) Capillary pressure

Fig. 5.7: Phase pressure and capillary pressure as functions of the overall molar density: nC_4 at $T = 360$ K, $r = 10$ nm and $\theta = \pi/6$.

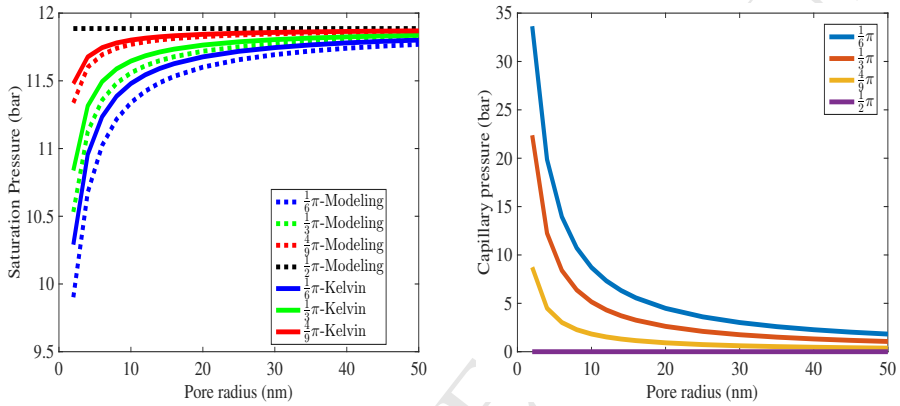

(a) Saturation pressure (b) Capillary pressure

Fig. 5.8: Saturation pressure and capillary pressure as functions of the pore radius: nC_4 at $n = 3$ kmol/m^3, $T = 360$ K and different contact angles.

is compressed with the increasing pore radiuses and contact angles since the overall molar density always keeps constant.

5.2. Binary mixture: CH_4 and nC_5. In this example, we consider a binary mixture composed of methane(CH_4) and pentane(nC_5) with mole fractions $z_{CH_4} = 0.35$ and $z_{nC_5} = 0.65$. The binary interaction coefficient between methane and pentane is 0.041. We simulate two-phase equilibria for this binary mixture at different conditions.

At the specified condition $T = 345$ K, $r = 10$ nm and $\theta = \pi/6$, the equilibrium state variables can be viewed as functions of the overall molar density. The phase density profiles of both components are illustrated in Figs. 5.11 and 5.12 respectively. The gas saturation profiles are shown in Figs. 5.13. The phase pressure and capillary pressure profiles are shown in Figs. 5.14(a) and 5.14(b). The corresponding results without capillary pressure are also depicted for comparison.

From Figs. 5.11 and 5.12, we can observe that owing to capillary effect, the liquid

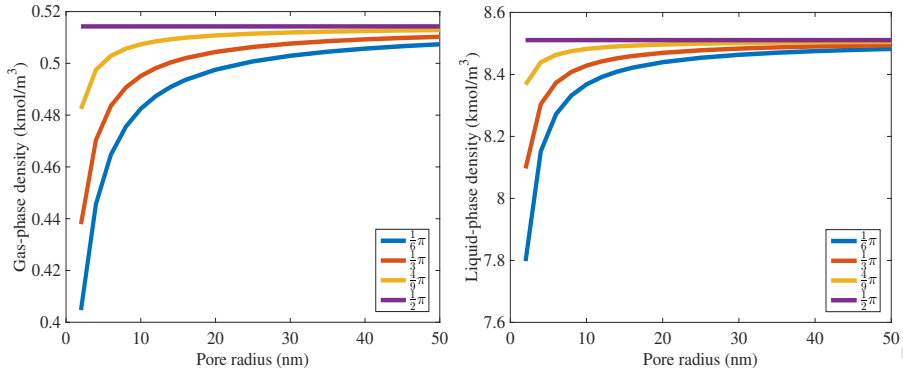

Fig. 5.9: Phase molar densities as functions of the pore radius: nC_4 at $n = 3$ kmol/m^3, $T = 360$ K and different contact angles.

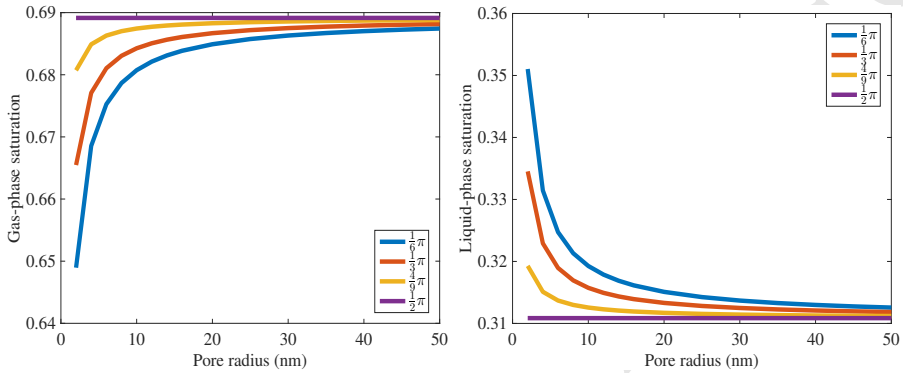

Fig. 5.10: Phase saturations as functions of the pore radius: nC_4 at $n = 3$ kmol/m^3, $T = 360$ K and different contact angles.

molar density of CH_4 becomes larger compared with the results in the absence of capillarity. This means that capillarity effect may make more of CH_4 dissolve into the liquid phase.

Fig. 5.14(a) depicts that both of gas and liquid pressures with capillarity effect are less than that without capillary pressure. From the results in Figs. 5.13 and 5.14(b), we apparently observe that as the overall molar density increases, the gas-phase saturation becomes smaller, and meanwhile, the capillary pressure also becomes weaker.

The phase equilibria are simulated at the specified condition $n = 5$ kmol/m^3, $r = 10$ nm and $\theta = \pi/6$, and in this case, the state variables are viewed as functions of the temperature. The phase density and saturation profiles are illustrated in Figs. 5.15(a) and 5.15(b) respectively. It is observed that due to the temperature rise, an increase of gas-phase molar density and a decrease of liquid-phase molar density take place as expected, but the liquid phase is expanding in the volume. The molar fraction profiles of each component are depicted in Figs. 5.16(a) and 5.16(b) respectively, which show that as the temperature increases, more methane may dissolve into the liquid phase, while pentane is increasingly evaporated into the gas phase. The phase pressure and capillary pressure profiles are shown in Figs. 5.17(a) and 5.17(b) respectively, and from these results, we still observe that the capillary pressure decreases with increasing temperature.

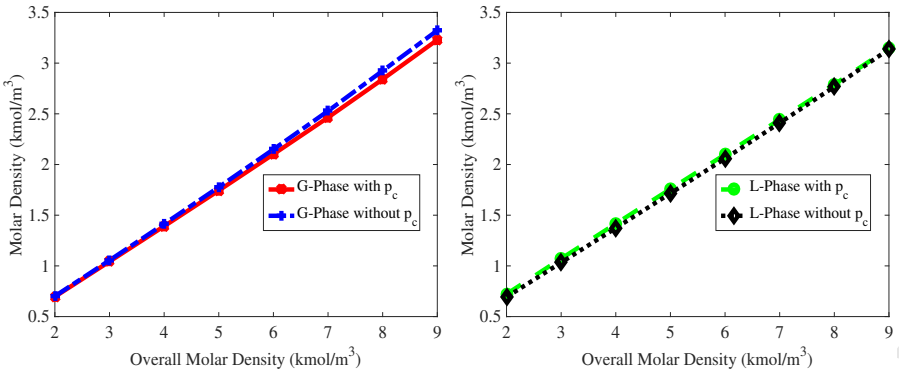

Fig. 5.11: Phase molar densities as functions of the overall molar density: CH_4 of the binary mixture at $T = 345$ K, $r = 10$ nm and $\theta = \pi/6$.

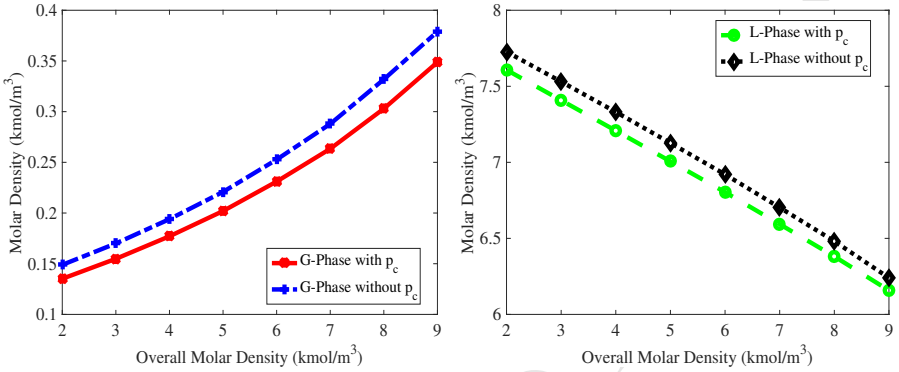

Fig. 5.12: Phase molar densities as functions of the overall molar density: nC_5 of the binary mixture at $T = 345$ K, $r = 10$ nm and $\theta = \pi/6$.

The phase equilibria at $n = 5$ kmol/m^3, $T = 380$ K and different contact angles are simulated, and for specified overall molar density, temperature and contact angle, the equilibrium state variables vary with the pore radius. We illustrate the saturation pressure profiles in Fig. 5.18(a), and we also depict the saturation pressures calculated by the Kelvin equation. We can see that for this binary mixture, the simulated saturation pressures are in agreement with the Kelvin equation in the envelopes at various contact angles. The capillary pressure profile is shown in Fig. 5.18(b), which demonstrates that the capillary pressure decreases with the pore radius, still being consistent with Young-Laplace equation.

The phase density and saturation profiles are illustrated in Figs. 5.19 and 5.20 respectively. We can obtain the observations similar to the pure substance that molar densities of both phases increase with the pore radius and contact angle, and as a result of the constant overall molar density, the liquid volume is compressed with the increased pore radiuses and contact angles.

6. Conclusions. A dynamical model for phase equilibria involving capillary pressure at specified moles, volume and temperature is derived by using the laws of thermodynamics and Onsager's reciprocal principle. This model has a set of unified formulations for both pure substances and multi-component mixtures, which describe the evolutionary process from a non-equilibrium state to an equilibrium state. Based

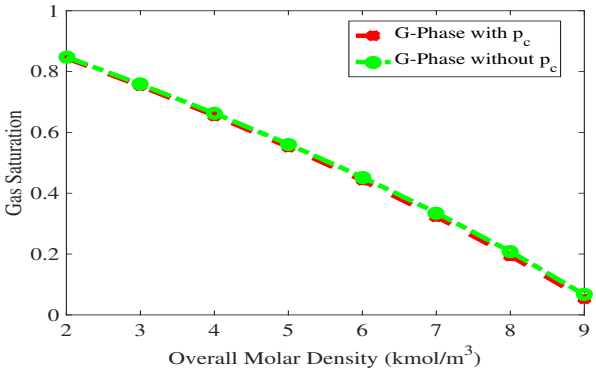

Fig. 5.13: Gas saturation as a function of the overall molar density: the binary mixture at $T = 345$ K, $r = 10$ nm and $\theta = \pi/6$.

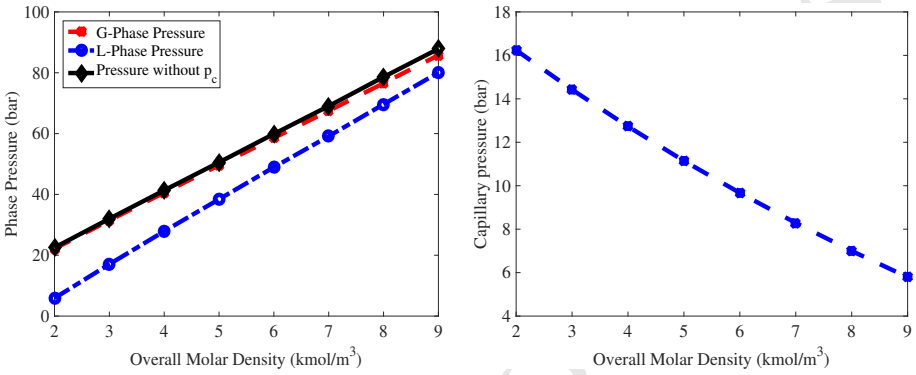

(a) Phase pressure (b) Capillary pressure

Fig. 5.14: Phase pressure and capillary pressure as functions of the overall molar density: the binary mixture at $T = 345$ K, $r = 10$ nm and $\theta = \pi/6$.

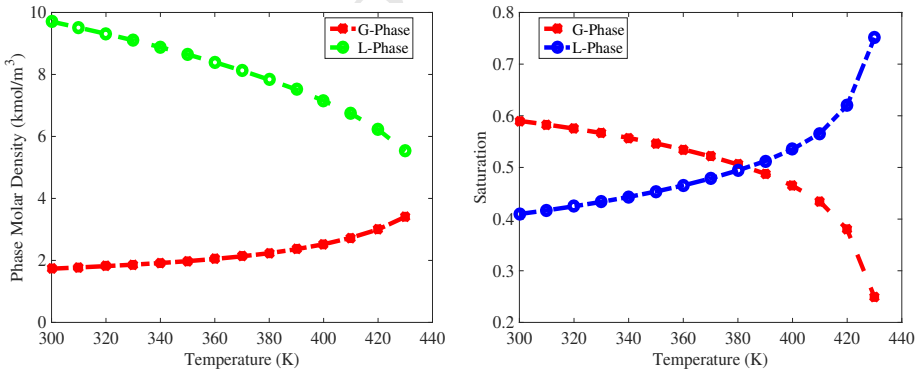

(a) Phase molar density (b) Phase saturation

Fig. 5.15: Phase molar density and phase saturation as functions of the temperature: the binary mixture at $n = 5$ kmol/m^3, $r = 10$ nm and $\theta = \pi/6$.

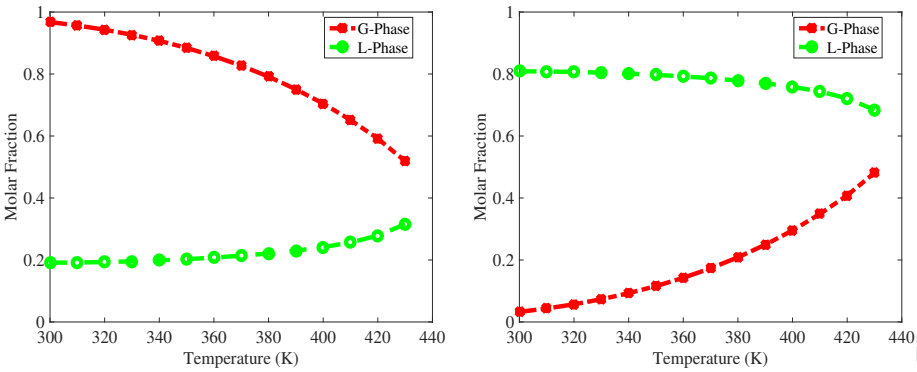

(a) Molar fraction of CH_4 (b) Molar fraction of nC_5

Fig. 5.16: Molar fractions as functions of the temperature: the binary mixture at $n = 5$ kmol/m^3, $r = 10$ nm and $\theta = \pi/6$.

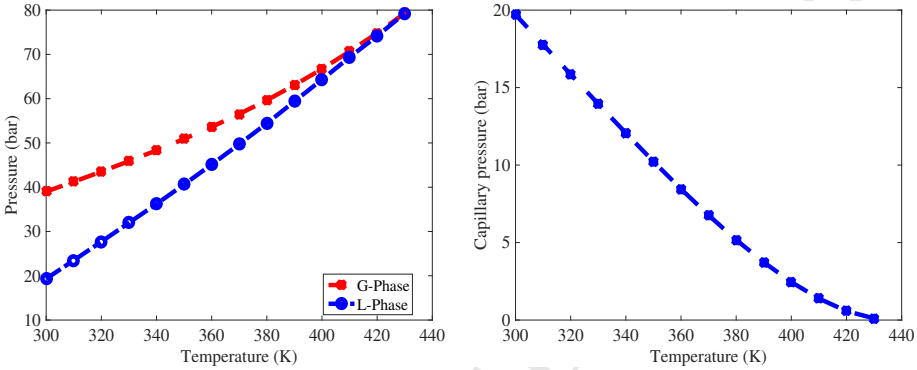

(a) Phase pressure (b) Capillary pressure

Fig. 5.17: Phase pressure and capillary pressure as functions of the temperature: the binary mixture at $n = 5$ kmol/m^3, $r = 10$ nm and $\theta = \pi/6$.

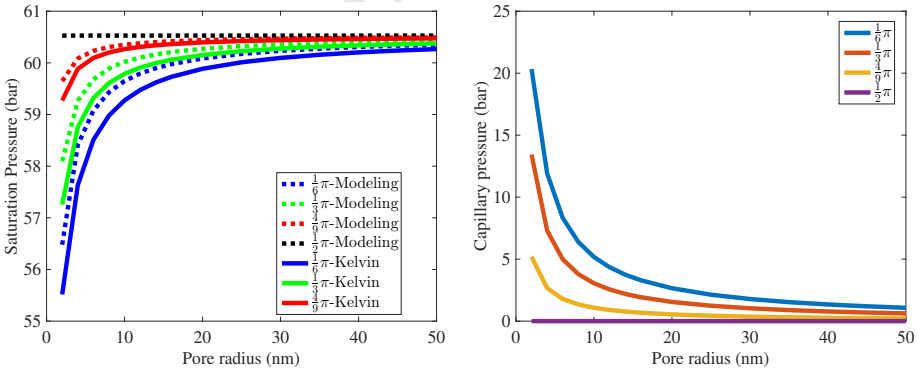

(a) Saturation pressure (b) Capillary pressure

Fig. 5.18: Saturation and capillary pressures as functions of the pore radius: the binary mixture at $n = 5$ kmol/m^3, $T = 380$ K and different contact angles.

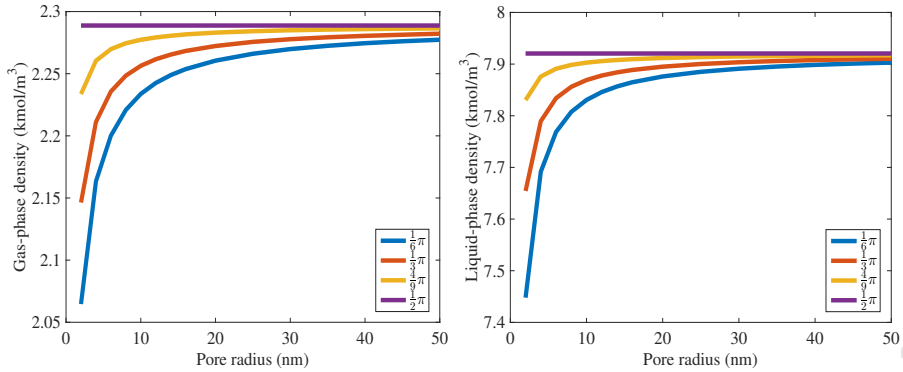

Fig. 5.19: Phase molar densities as functions of the pore radius: the binary mixture at $n = 5$ kmol/m^3, $T = 380$ K and different contact angles.

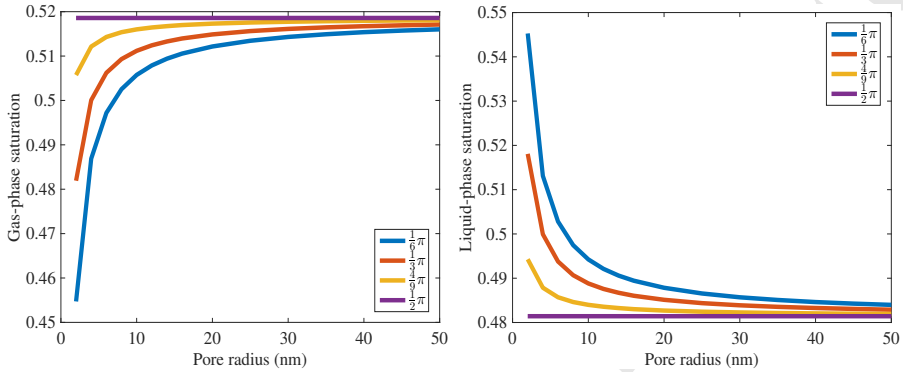

Fig. 5.20: Phase saturations as functions of the pore radius: the binary mixture at $n = 5$ kmol/m^3, $T = 380$ K and different contact angles.

on the convex-concave splitting of the total Helmholtz energy, an efficient, thermodynamically stable numerical algorithm is developed to simulate the dynamical model. We derive a phase stability condition in the presence of capillarity effect at the NVT condition, and moreover, we propose a stable numerical algorithm for the phase stability testing, which can provide the feasible initial conditions. The proposed method is used to calculate the phase equilibria for the pure-substance and mixture systems with capillarity under the NVT condition. The proposed model and simulation method show promises in two-phase flow in porous media in the future.

Appendix A. Helmholtz free energy density.

In this appendix, we describe the formulation of Helmholtz free energy density $f(\mathbf{n})$ of a homogeneous fluid and the parameters used in Peng-Robinson equation of state. The Helmholtz free energy density $f(\mathbf{n})$ can be expressed as

$$f(\mathbf{n}) = f^{\text{ideal}}(\mathbf{n}) + f^{\text{repulsion}}(\mathbf{n}) + f^{\text{attraction}}(\mathbf{n}),$$

$$f^{\text{ideal}}(\mathbf{n}) = RT \sum_{i=1}^{M} n_i \left(\ln n_i - 1\right),$$

$$f^{\text{repulsion}}(\mathbf{n}) = -nRT \ln\left(1 - bn\right),$$

$$f^{\text{attraction}}(\mathbf{n}) = \frac{a(T)n}{2\sqrt{2}b} \ln\left(\frac{1+(1-\sqrt{2})bn}{1+(1+\sqrt{2})bn}\right),$$

where $n = \sum_{i=1}^{M} n_i$, T is the temperature and R stands for the universal gas constant. Here, $a(T)$ and b are the energy parameter and the covolume, respectively, which can be calculated on the basis of the mixture composition, temperature, critical temperature and critical pressure. We denote by T_{c_i} and P_{c_i} the critical temperature and critical pressure of component i, respectively. For the ith component, we denote the reduced temperature by $T_{r_i} = T/T_{c_i}$. The parameters a_i and b_i are calculated as

$$a_i = 0.45724\frac{R^2T_{c_i}^2}{P_{c_i}}\left[1+m_i(1-\sqrt{T_{r_i}})\right]^2, \quad b_i = 0.07780\frac{RT_{c_i}}{P_{c_i}}.$$

The coefficients m_i are computed through the following formulations

$$m_i = 0.37464 + 1.54226\omega_i - 0.26992\omega_i^2, \quad \omega_i \leq 0.49,$$

$$m_i = 0.379642 + 1.485030\omega_i - 0.164423\omega_i^2 + 0.016666\omega_i^3, \quad \omega_i > 0.49,$$

where ω_i represents the acentric factor. For a mixture, we let k_{ij} be the given binary interaction coefficients for the energy parameters, and we use the mixing rules to calculate $a(T)$ and b as

$$a(T) = \sum_{i=1}^{M}\sum_{j=1}^{M} y_i y_j \left(a_i a_j\right)^{1/2}(1-k_{ij}), \quad b = \sum_{i=1}^{M} y_i b_i,$$

where $y_i = n_i/n$ is the mole fraction of component i.

The Peng-Robinson equation of state (PR-EOS) [27] has the following form:

$$p = \frac{RT}{v-b} - \frac{a(T)}{v(v+b)+b(v-b)},$$

where p is the pressure and v is the molar volume.

Appendix B. Interfacial tension.

The Weinaug–Katz correlation [39] is employed to calculate the interfacial tension:

$$\sigma^{1/4} = \sum_{i=1}^{M} [\boldsymbol{P}]_i \left(n_i^L - n_i^G\right),$$

where $[\boldsymbol{P}]_i$ is the parachor of component i.

Appendix C. Kelvin equation.

The Kelvin equation reveals that the vapor pressure decreases with increasing interface curvature. Its classical form can be written as [6]:

$$p_G = p_\infty \exp\left(-\frac{p_c v^L}{RT}\right), \tag{C.1}$$

where p_∞ is the saturated vapor pressure, $p_c = \frac{2\sigma\cos\theta}{r}$ is the capillary pressure, and v^L is the molar volume of the liquid.

We note that (C.1) is originally derived for a single-component fluid. The above classical Kelvin equation has been generalized in [31] for non-ideal fluids, especially for a multicomponent non-ideal mixture. The generalized Kelvin equation for a non-ideal multicomponent mixture proposed in [31] has a different and complicate form compared with its classical form and the equation for a single component. For sake of simplification to exhibit the relationship between the vapor pressure and pore radius in numerical tests of this work, we assume that the tested multicomponent mixture behaves approximately as a pure substance, so we still apply the classical Kelvin equation (C.1) to approximate the case of the multicomponent mixture (v^L is taken as the liquid-phase molar volume of the multicomponent mixture).

Acknowledgement. The authors would like to thank the anonymous reviewers for their constructive suggestions and comments to improve the original version of this paper.

REFERENCES

[1] T. Babadagli, C. U. Hatiboglu, T. Hamida. Evaluation of Matrix-Fracture Transfer Functions for Counter-Current Capillary Imbibition. *Transport in Porous Media*, 80:17–56, 2009.

[2] E. M. Blokhuis and J. Kuipers. Thermodynamic expressions for the Tolman length. *Journal of Chemical Physics*, 124, 074701, 2006.

[3] Z. Chen, G. Huan, Y. Ma, Computational methods for multiphase flows in porous media. SIAM Comp. Sci. Eng., Philadelphia, 2006.

[4] D. J. Eyre. Unconditionally gradient stable time marching the Cahn-Hilliard equation. *Computational and mathematical models of microstructural evolution (San Francisco, CA, 1998),* Mater. Res. Soc. Sympos. Proc., 529: 39–46. MRS, Warrendale, PA, 1998.

[5] X. Fan, J. Kou, Z. Qiao, S. Sun. A Componentwise Convex Splitting Scheme for Diffuse Interface Models with Van der Waals and Peng–Robinson Equations of State. *SIAM Journal on Scientific Computing,* 39(1): B1–B28, 2017.

[6] A. Firoozabadi. *Thermodynamics of hydrocarbon reservoirs.* McGraw-Hill New York, 1999.

[7] S. R. De Groot, P. Mazur. *Non-Equilibrium Thermodynamics.* Dover Publications, New York, 2011.

[8] T. Jindrová, J. Mikyška. Fast and robust algorithm for calculation of two-phase equilibria at given volume, temperature, and moles. *Fluid Phase Equilibria*, 353:101–114, 2013.

[9] T. Jindrová, J. Mikyška. General algorithm for multiphase equilibria calculation at given volume, temperature, and moles. *Fluid Phase Equilibria*, 393:7–25, 2015.

[10] C. K. Ho, B. W. Arnold, S. J. Altman. Dual-Permeability Modeling of Capillary Diversion and Drift Shadow Effects in Unsaturated Fractured Rock. *Journal of Heat Transfer*, 131, 101012, 2009.

[11] J. Kou, S. Sun, X. Wang. Efficient numerical methods for simulating surface tension of multicomponent mixtures with the gradient theory of fluid interfaces. *Computer Methods in Applied Mechanics and Engineering*, 292: 92–106, 2015.

[12] J. Kou, S. Sun. Numerical methods for a multi-component two-phase interface model with geometric mean influence parameters. *SIAM Journal on Scientific Computing*, 37(4): B543–B569, 2015.

[13] J. Kou, S. Sun. Unconditionally stable methods for simulating multi-component two-phase interface models with Peng-Robinson equation of state and various boundary conditions. *Journal of Computational and Applied Mathematics*, 291(1): 158–182, 2016.

[14] J. Kou, S. Sun, X. Wang. An energy stable evolution method for simulating two-phase equilibria of multi-component fluids at constant moles, volume and temperature. *Computational Geosciences*, 20: 283–295, 2016.

[15] J. Kou, S. Sun. Efficient energy-stable dynamic modeling of compositional grading. *International Journal of Numerical Analysis and Modeling*, 14(2):218–242, 2017.

[16] L. W. Lake. *Fundamentals of enhanced oil recovery.* Society of Petroleum Engineers, 1986.

[17] M. L. Michelsen. The isothermal flash problem. part i. stability. *Fluid Phase Equilibria*, 9(1):1–19, 1982.

[18] M. L. Michelsen. The isothermal flash problem. part ii. phase-split calculation. *Fluid Phase Equilibria*, 9(1):21–40, 1982.

[19] M. L. Michelsen. State function based flash specifications. *Fluid Phase Equilibria*, 158–160: 617–626, 1999.

[20] M. L. Michelsen, J. M. Mollerup. *Thermodynamic models: fundamentals & computational aspects*. Tie-Line Publications Denmark, 2004.

[21] J. Mikyška, A. Firoozabadi. A new thermodynamic function for phase-splitting at constant temperature, moles, and volume. *AIChE Journal*, 57(7):1897–1904, 2011.

[22] J. Mikyška, A. Firoozabadi. Investigation of mixture stability at given volume, temperature, and number of moles. *Fluid Phase Equilibria*, 321:1–9, 2012.

[23] C. Miqueu, B. Mendiboure, C. Graciaa, J. Lachaise. Modelling of the surface tension of binary and ternary mixtures with the gradient theory of fluid interfaces. *Fluid Phase Equilibria*, 218:189–203, 2004.

[24] X. Mu, F. Frank, F. O. Alpak, W. G. Chapman. Stabilized density gradient theory algorithm for modeling interfacial properties of pure and mixed systems. *Fluid Phase Equilibria*, 435: 118–130, 2017.

[25] N.R. Nagarajan, A.S. Cullick. New strategy for phase equilibrium and critical point calculations by thermodynamic energy analysis. Part I. Stability analysis and flash. *Fluid Phase Equilibria*, 62(3): 191–210, 1991.

[26] B. Nojabaei, R.T. Johns, L. Chu. Effect of Capillary Pressure on Phase Behavior in Tight Rocks and Shales. *SPE Reservoir Evaluation and Engineering*, 16: 281–289, 2013.

[27] D. Peng, D. B. Robinson. A new two-constant equation of state. *Industrial and Engineering Chemistry Fundamentals*, 15(1):59–64, 1976.

[28] O. Polívka, J. Mikyška. Compositional modeling in porous media using constant volume flash and flux computation without the need for phase identification. *Journal of Computational Physics*, 272:149–169, 2014.

[29] Z. Qiao, S. Sun. Two-phase fluid simulation using a diffuse interface model with Peng-Robinson equation of state. *SIAM Journal on Scientific Computing*, 36(4): B708–B728, 2014.

[30] D. R. Sandoval, W. Yan, M. L. Michelsen, E. H. Stenby. The Phase Envelope of Multicomponent Mixtures in the Presence of a Capillary Pressure Difference. *Industrial and Engineering Chemistry Research*, , 55 (22): 6530–6538, 2016.

[31] A. A. Shapiro, E. H. Stenby. Kelvin equation for a non-ideal multicomponent mixture. *Fluid Phase Equilibria*, 134: 87–101, 1997.

[32] J. Shen, X. Yang. Decoupled, energy stable schemes for phase-field models of two-phase incompressible flows. *SIAM Journal on Numerical Analysis,* 53(1): 279-296, 2015.

[33] M. Sherafati, K. Jessen. Stability analysis for multicomponent mixtures including capillary pressure. *Fluid Phase Equilibria*, 433: 56–66, 2017.

[34] K. S.W. Sing, R. T. Williams. Historical aspects of capillarity and capillary condensation. *Microporous and Mesoporous Materials*, 154: 16–18, 2012.

[35] T. Smejkal, J. Mikyška. Phase stability testing and phase equilibrium calculation at specified internal energy, volume, and moles. *Fluid Phase Equilibria,* 431: 82–96, 2017.

[36] B. C. Stimpson, M. A. Barrufet. Thermodynamic modeling of pure components including the effects of capillarity. *J. Chem. Eng. Data*, 61: 2844–2850, 2016.

[37] S. P. Tan, M. Piri. Equation-of-state modeling of confined-fluid phase equilibria in nanopores. *Fluid Phase Equilibria*, 393: 48–63, 2015.

[38] S. M. Wise, C. Wang, J. S. Lowengrub. An energy-stable and convergent finite-difference scheme for the phase field crystal equation. *SIAM J. Numer. Anal.,* 47(3): 2269–2288, 2009.

[39] C. F. Weinaug, D. L. Katz. Surface tensions of methane-propane mixtures. *Industrial and Engineering Chemistry*, 35(2): 239–246, 1943.